united nations educational, scientific and cultural organization

international atomic energy agency

the
abdus salam
international centre for theoretical physics

SMR.1320 - 24

SUMMER SCHOOL
on
LOW-DIMENSIONAL QUANTUM SYSTEMS:
Theory and Experiment
(16 - 27 JULY 2001)

PLUS

PRE-TUTORIAL SESSIONS
(11 - 13 JULY 2001)

SINGLE-WALL CARBON NANOTUBES

S. GOGOLIN
Imperial College of Science & Technology
Department of Physics
London, SW7 2BZ
U.K.

These are preliminary lecture notes, intended only for distribution to participants

Single-wall Carbon Nanotubes

Sasha Gogolin

Imperial College London, Math Dept

Collaboration: Egger, Komnik

Plan:

- preliminaries
- making of tubes
- interaction effects
- conductance experiments
- field emission

- **Graphite**

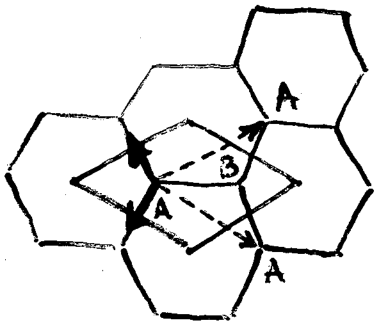

$[cc] = d = 1.42\,\mathring{A}$

$a = \sqrt{3}\,d$

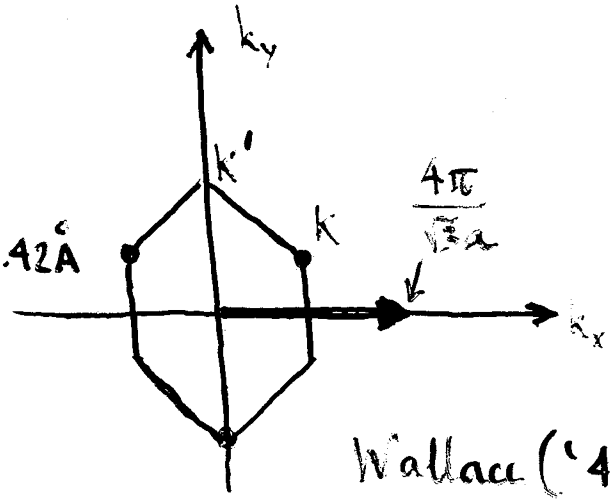

$n_1\vec{a}_1 + n_2\vec{a}_2$, $\vec{a}_{1,2} = \left(\frac{\sqrt{3}}{2}a, \pm\frac{1}{2}a\right)$

Wallace ('47)

$$H = \gamma_0 \sum_{n}\left[A^+_{\vec{n}} B_{\vec{n}} + A^+_{n_1+1,n_2} B_{\vec{n}} + A^+_{n_1,n_2+1} B_{\vec{n}}\right] + \text{H.c.} =$$

$$= \gamma_0 \sum_{\vec{k}} \underbrace{\left[1 + 2e^{i\frac{\sqrt{3}}{2}k_x a}\cos\left(\frac{k_y a}{2}\right)\right]}_{h_{\vec{k}}} A^+_{\vec{k}} B_{\vec{k}} + \text{H.c.} \rightarrow \begin{bmatrix} 0 & h_{\vec{k}} \\ h^*_{\vec{k}} & 0 \end{bmatrix}$$

$$E_{2D}(\vec{k}) = \pm |h_{\vec{k}}|^2 = \pm\gamma_0 \left\{1 + 4\cos\left(\frac{\sqrt{3}k_x a}{2}\right)\cos\left(\frac{k_y a}{2}\right) + 4\cos^2\left(\frac{k_y a}{2}\right)\right\}^{1/2}$$

Around K-points $\vec{k} = \vec{K} + \vec{q}$ and $\underline{E_{2D}(\vec{q}) = \pm \hbar v |\vec{q}|}$

2D Dirac

$v = 8\cdot 10^5$ m/s

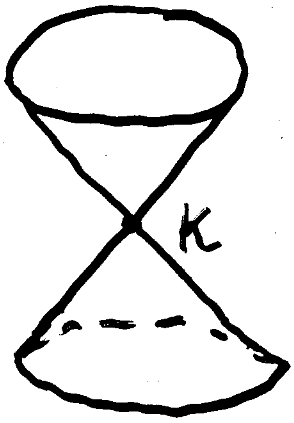

Magnetic field H $\perp$ plane

Rammal, J Phys. (1985)

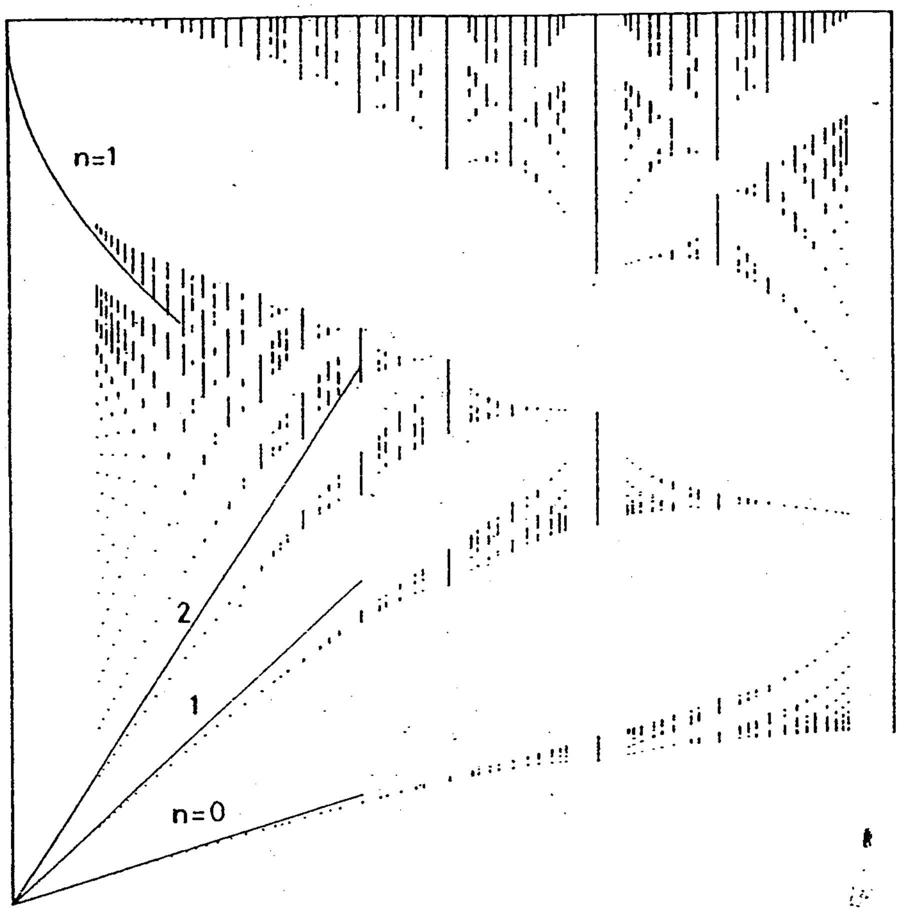

Fig. 4. — Energy spectrum for broadened Landau levels.

Phase factor

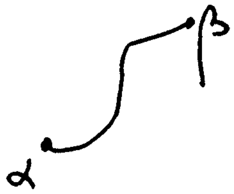

$$\gamma_{\alpha\beta} = \frac{2\pi}{\phi_0} \int_\alpha^\beta \vec{A}\,d\vec{\ell}$$

$\Rightarrow$ diference equations $\Rightarrow$ linearisation around Dirac point

$\Rightarrow$ spectrum: $E^2 \simeq \sqrt{3}\,\gamma\, n$ (Landau levels)

$n = 1, 2, 3, \ldots$

$\gamma = 2\pi\phi/\phi_0$, $\phi = \frac{3\sqrt{3}}{2} H a_0^2$

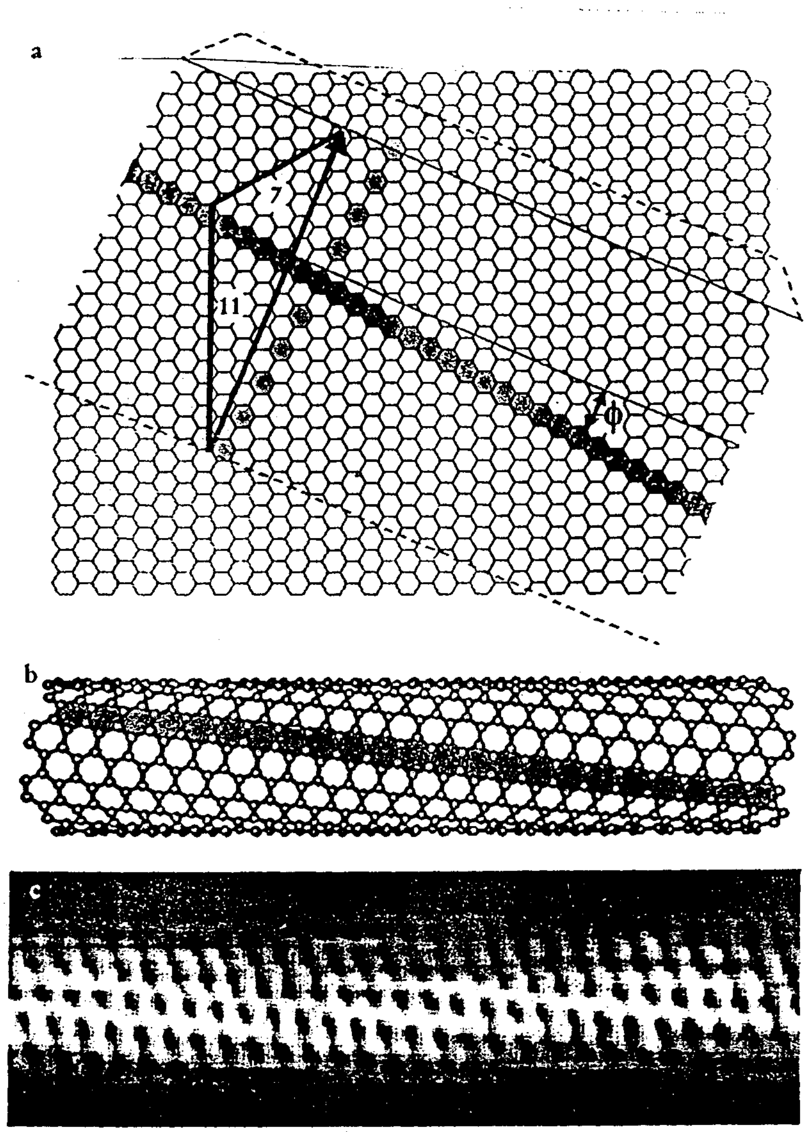

FIGURE 1. HOW TO WRAP A NANOTUBE a single sheet of graphite. First, copy the part (a) onto a transparent overhead shee (This panel can also be downloaded from http://vortex.tn.tudelft.nl/~pt on the w Second, cut out the part of the sheet indi by the dashed lines. Third, fold up the cu part so that the blue arrow's tail coincide its head. Match the hexagons on the over tab carefully to those on the tube body. Finally, fasten the tube together with transparent tape. A nanotube with indice (11,7) now has been formed. The indices describe the projection of the circumfere vector (the blue arrow) onto the basis ve of the graphite lattice, as shown. The red illustrates the winding of hexagons along tube direction. It forms the angle Φ (the angle) with respect to the tube axis. Wra the sheet along the yellow or green hexa rows instead of along the blue vector lea (n,0) "zigzag" tubes (so named because o rows of alternating carbon bonds around circumference) or (n,n) "armchair" tubes hexagon rows parallel to the tube axis, respectively. The indices (n,m) are crucia important for the electronic properties o nanotubes: Tubes for which $n - m = 3i$, an integer, are metallic; all others are semiconducting. (b) Atomic structure of t nanotube that results from the folding abo (Image courtesy of Philippe Lambin, Univ of Namur.) (c) Atomically resolved scanni tunneling microscope image of a nanotube (Adapted from Wildöer *et al.*, ref. 6.)

ergy k_BT, about 0.025 eV. Only tw one-dimensional subbands cross the energy in metallic nanotubes; all the through such tubes is therefore pred be carried by only this pair of su Because each subband can in princi port a conductance of $G_0 = 2e^2/h$ (t

4

$$k_x^{n} = \frac{n}{N}\,\frac{2\pi}{\sqrt{3}a}$$

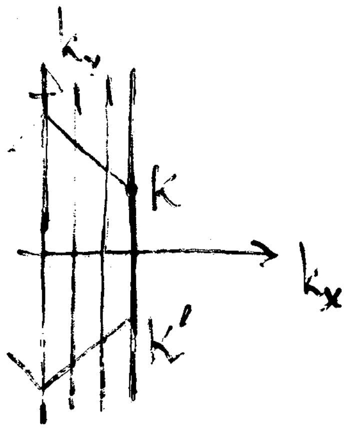

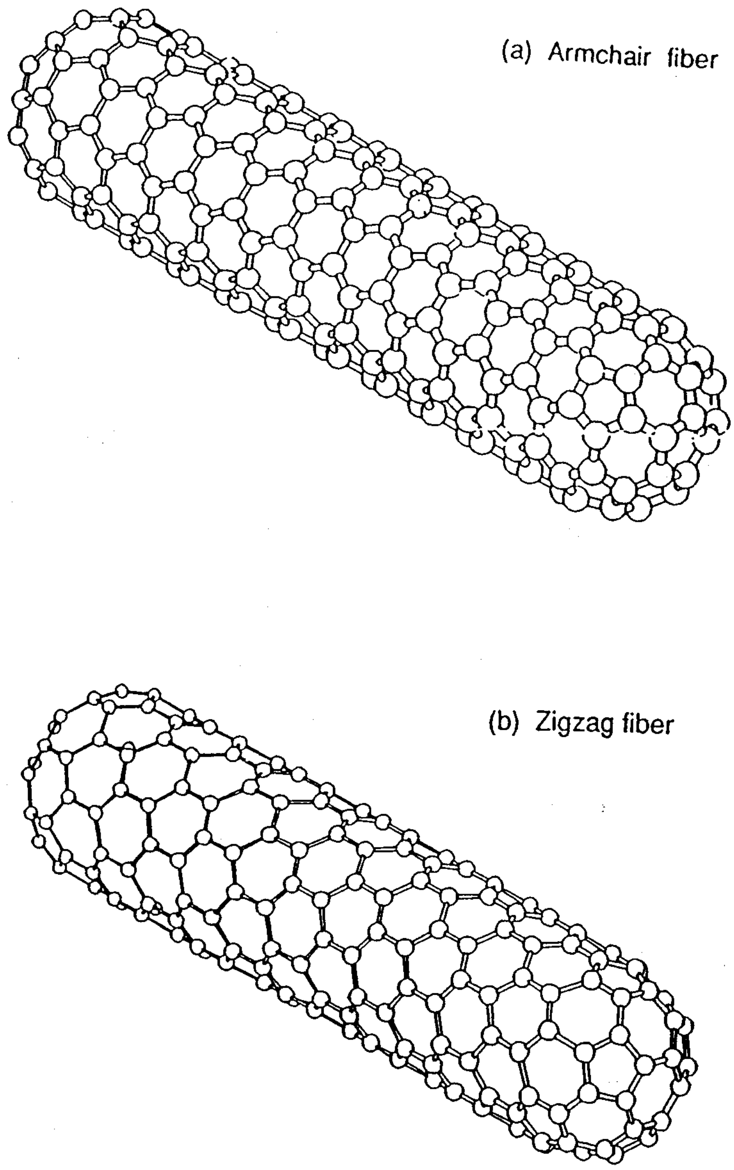

FIG. 2. Atomic arrangements of carbon atoms in the (a armchair fiber and (b) zigzag fiber.

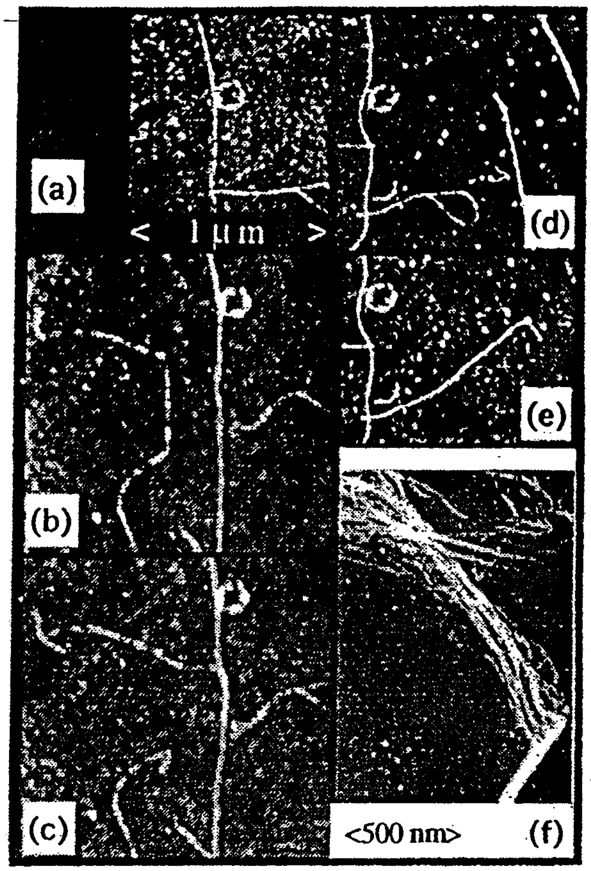

FIG. 1. Circuit fabrication using AFM manipulation. The scale is the sa
for each figure. (a) We begin with one vertical tube (main tube) and
horizontal tube (lasso tube). (b) A tube is brought in close proximity to
main tube. (c) The tube is pushed against (perhaps on top of) the main tu
(d) Additional tubes are manipulated on top of the main tube. A piece
nanotube was broken off and sits near the lasso tube. (e) The lasso tube
opened and unwanted tubes pushed away. (f) AFM manipulation cau
SWNT bundles to unravel.

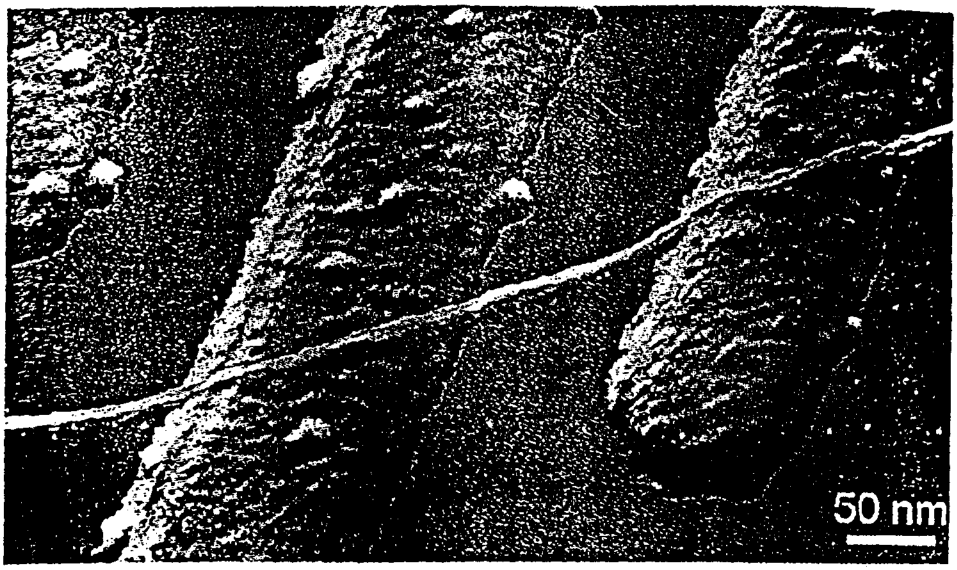
50 nm

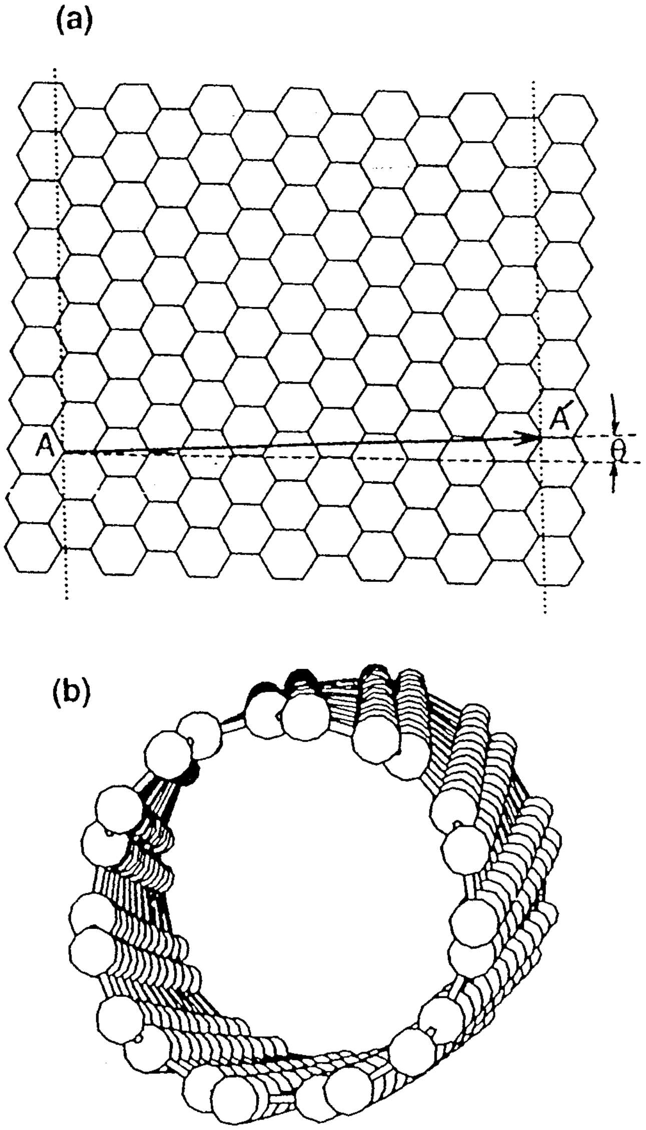

FIG. 3. (a) The vector $\overrightarrow{AA'}$ specifies a chiral fiber. We connect two dotted lines, normal to $\overrightarrow{AA'}$ at A and A', to form a chiral fiber. (b) Atomic arrangement of the corresponding chiral fiber. The vector specifying an armchair has $\theta = 0°$ and a zigzag fiber has $\theta = 30°$.

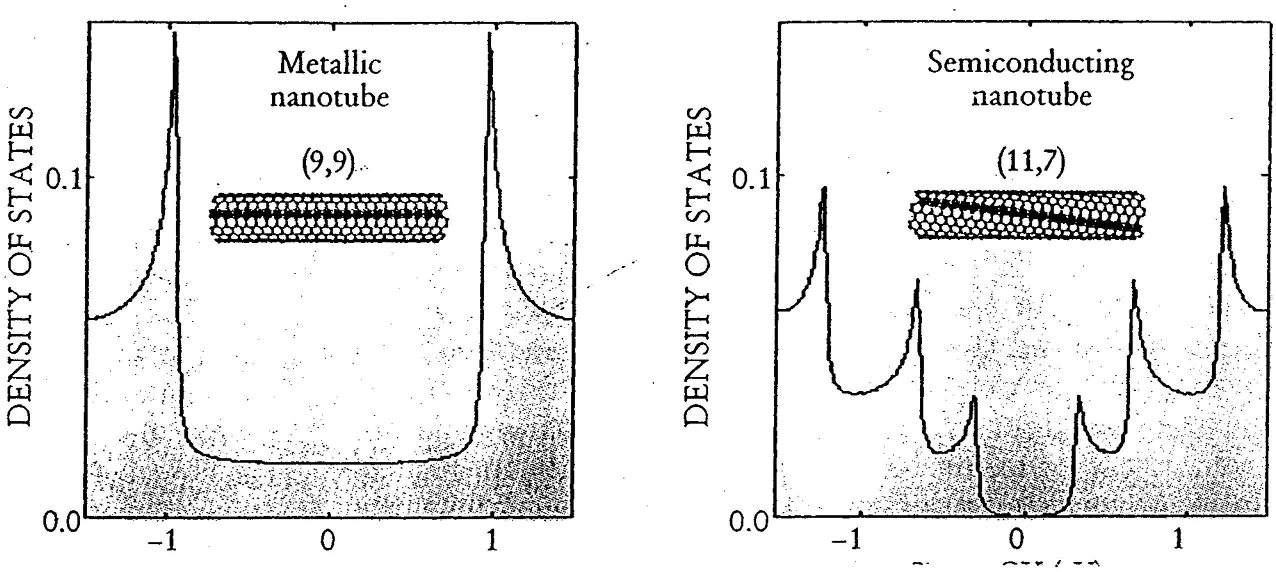
DENSITY OF STATES
0.1
0.0
Metallic
nanotube
(9,9)
-1
0
1
DENSITY OF STATES
0.1
0.0
Semiconducting
nanotube
(11,7)
-1
0
1

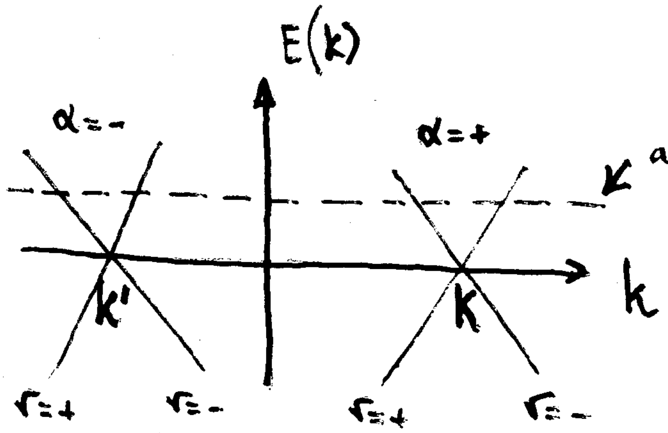

away from half filling
(~100meV)

$$\Psi_\sigma(\vec r) = \sum_{r\alpha} \varphi_{r\alpha}(\vec r)\,\psi_{r\alpha\sigma}(x)$$

1D electron operators

$$H_0 = -iv\sum_{r\alpha\sigma} r\int dx\, \psi^+_{r\alpha\sigma}\,\partial_x\psi_{r\alpha\sigma}$$

and

$$H_{int} = \frac{1}{2}\sum_{\sigma\sigma'}\int d\vec r\, d\vec r'\, \Psi^+_\sigma(\vec r)\,\Psi^+_{\sigma'}(\vec r')\,U(\vec r-\vec r')\,\Psi_{\sigma'}(\vec r')\,\Psi_\sigma(\vec r)$$

$$H_{int} = \frac{1}{2}\sum_{rr'\sigma\sigma'}\ \sum_{\alpha_1\ldots\alpha_4}\int dx\,dx'\, V^{\{rr'\}}_{\{\alpha\}}(x-x')\,\psi^+_{r\alpha_1\sigma}(x)\,\psi^+_{r'\alpha_2\sigma'}(x')\,*$$

$$*\,\psi_{r'\alpha_3\sigma'}(x')\,\psi_{r\alpha_4\sigma}(x')$$

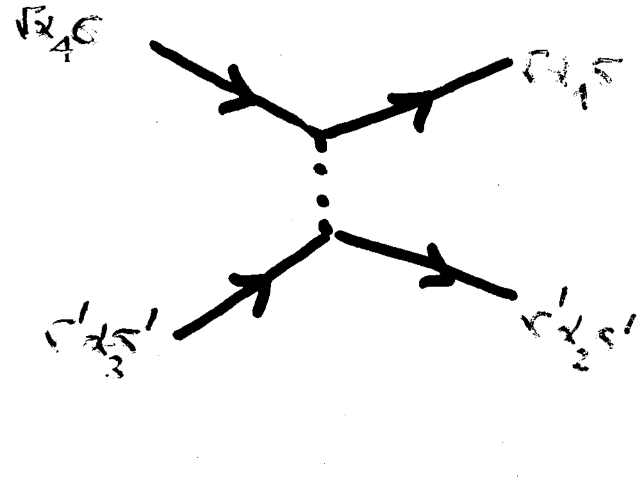

Egger and G ('97, '98)
Kane, Balents, MPA Fisher ('97)

Most important: forward scattering

$$H^{(0)}_{FS} = \frac{1}{2}\int dx\,dx'\,\rho(x)\,V(x-x')\,\rho(x')$$

total 1D density

$$\rho = \sum_{r\alpha\sigma} \psi^{+}_{r\alpha\sigma}\psi_{r\alpha\sigma}$$

$$V(k) = \frac{2e^2}{\varkappa}\ln\left(1/kR\right)$$

$(\varkappa \sim 1.5)$

$\boxed{\text{Other interactions are "irrelevant"}}$

<u>**Bosonization**</u> : $\psi_{r\alpha\sigma} \sim e^{iq_F r x + i k_F \alpha x + i\phi_{r\alpha\sigma}}$

$$\begin{cases} \phi_{c+} = \frac{1}{2}\sum_{r\alpha\sigma}\varphi_{r\alpha\sigma} & \leftarrow \text{total charge} \\ \phi_{c-} = \frac{1}{2}\sum_{r\alpha\sigma}\alpha\varphi_{r\alpha\sigma} & \leftarrow \text{charge flavour} \\ \phi_{s+} = \frac{1}{2}\sum_{r\alpha\sigma}\sigma\varphi_{r\alpha\sigma} & \leftarrow \text{total spin} \\ \phi_{s-} = \frac{1}{2}\sum_{r\alpha\sigma}\alpha\sigma\varphi_{r\alpha\sigma} & \leftarrow \text{spin flavour} \end{cases}$$

$$\rho(x) = \frac{2}{\sqrt{\pi}}\partial_x\phi_{c+}$$

The LL tube Hamiltonian:

$$H = \frac{1}{2} \sum_{j=c\pm, s\pm} u_j \int dx \left[K_j \Pi_j^2 + \frac{1}{K_j} (\partial \phi_j)^2 \right] ; \quad u_j = v/K_j$$

$$K_{c-} = K_{s\pm} = 1 ; \quad K_{c+} = K = \left[1 + \frac{8e^2}{\pi v \varkappa} \ln\left(\frac{L}{R}\right) \right]^{-1/2}$$

the LL parameter for a nanotube

Nanotube = (renormalised plasmon) + + (3 free bosons)

Charging energy: $E_c = \frac{1}{2L^2} \int dx\, dx' \frac{e^2}{\varkappa |x-x'|} \simeq \frac{e^2}{\varkappa L} \ln\left(\frac{L}{R}\right)$

For Tans, et al (Nature '97), $E_c = 2.6\,meV$, $L = 3\,\mu m$ $\longmapsto$ $K \simeq 0.2$

Bockrath, et al (Nature '99), several device $\longmapsto$ $K \simeq 0.28$

From bosonization formulas for, $\psi \sim e^{i\varphi}$, follows that:

	Theory ($K=0.28$)	Experiment (Bockrath, et al '99)	
$\alpha_{bulk} = \frac{1}{8}\left(K + \frac{1}{K} - 2\right)$	0.24	0.3	($\div$ 0.05)
$\alpha_{edge} = \frac{1}{4}\left(\frac{1}{K} - 1\right)$	0.65	0.6	

Bockrath, et al '99
D. Cobden

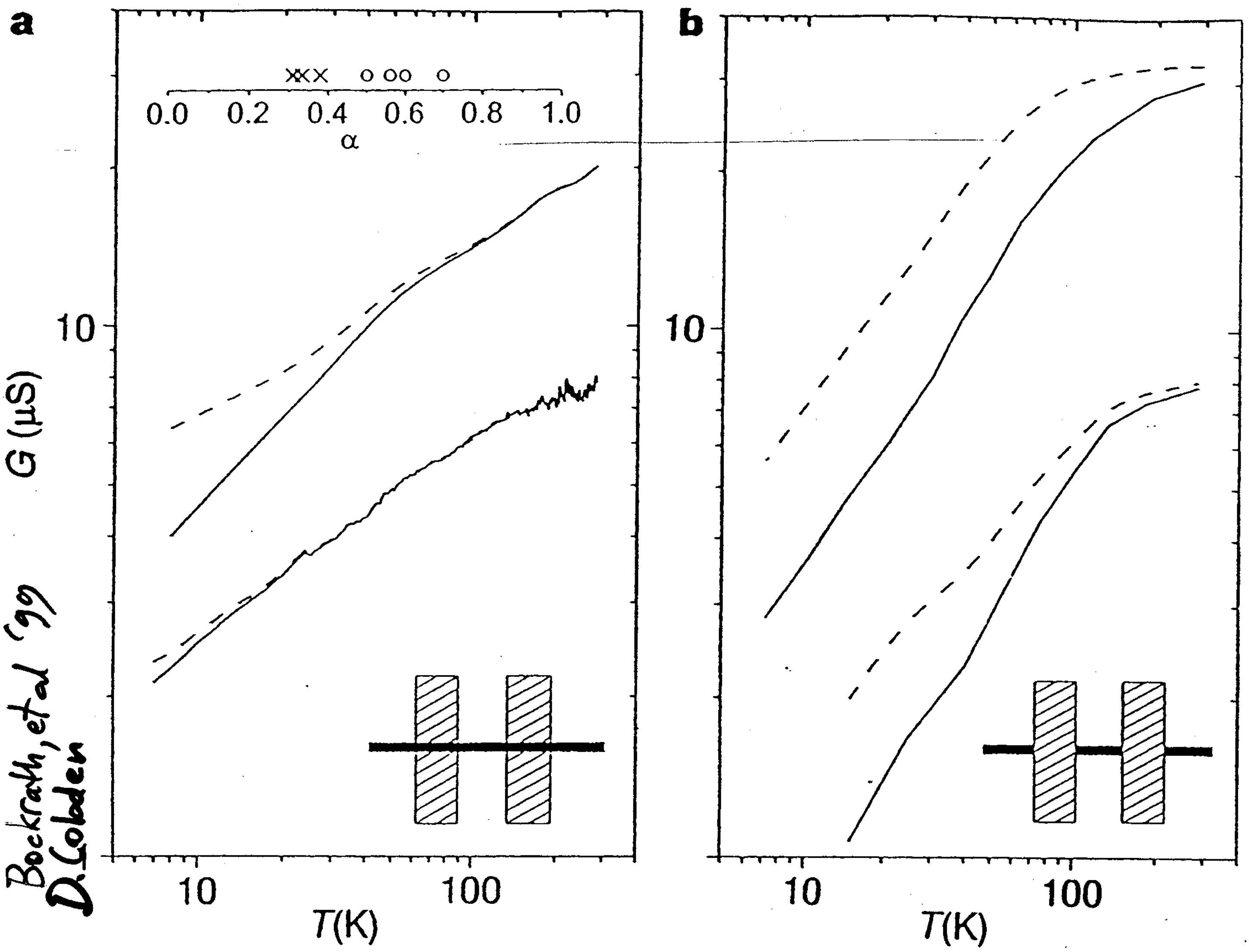

Figure 2 Conductance G plotted against temperature T for individual nanotube ropes. The data are plotted on a log–log scale. **a**, Data for ropes that are deposited over pre-defined leads (bulk-contacted); **b**, data for ropes that are contacted by evaporating the leads on top of the ropes (end-contacted). Sketches depicting the measurement configuration are shown in the lower insets. The plots show both the raw data (solid line) and the data corrected for the temperature dependence expected from the Coulomb blockade (CB) model (dashed line). We correct the data by dividing the measured $G(T)$ by the theoretically expected temperature dependence in the CB model. This correction factor depends only on U/k_BT, and, because U can be independently measured from the temperature dependence of the Coulomb oscillations, the correction procedure requires no adjustable

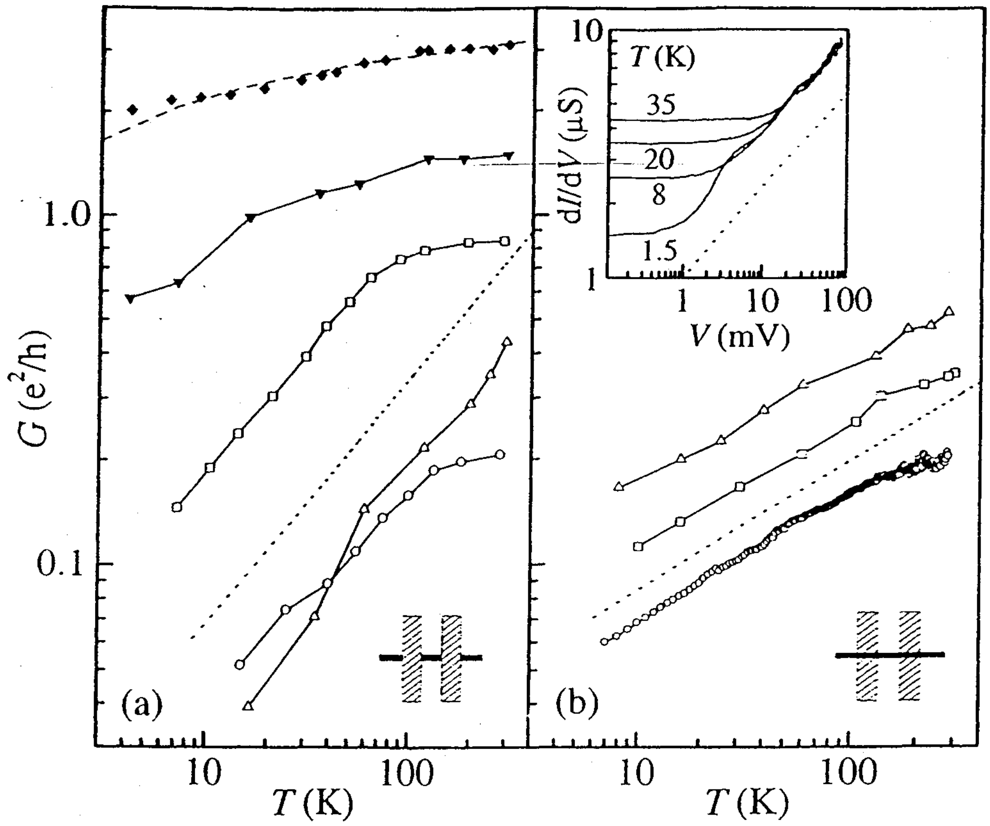

Fig. 7a,b. Conductance (averaged over V_g) vs. temperature for several devices. The data plotted with *open symbols* have been corrected for Coulomb blockade, whereas the others have not. a Metal-on-tube devices. The *open circles* correspond to the data in Fig. 3. The *dotted line* indicates $G \propto T^{0.7}$. The *dashed line* is a fit to $G = G_0 - aT^b$ with $G_0 = 4$, giving $b = -0.22$. **b** Tube-on-metal devices. The *dotted line* here indicates $G \propto T^{0.37}$. *Inset:* dI/dV vs. V at several temperatures for a tube-on-metal device. The *dotted line* here indicates $dI/dV \propto V^{0.37}$

Nygard, et al '99

Bockrath et al '99

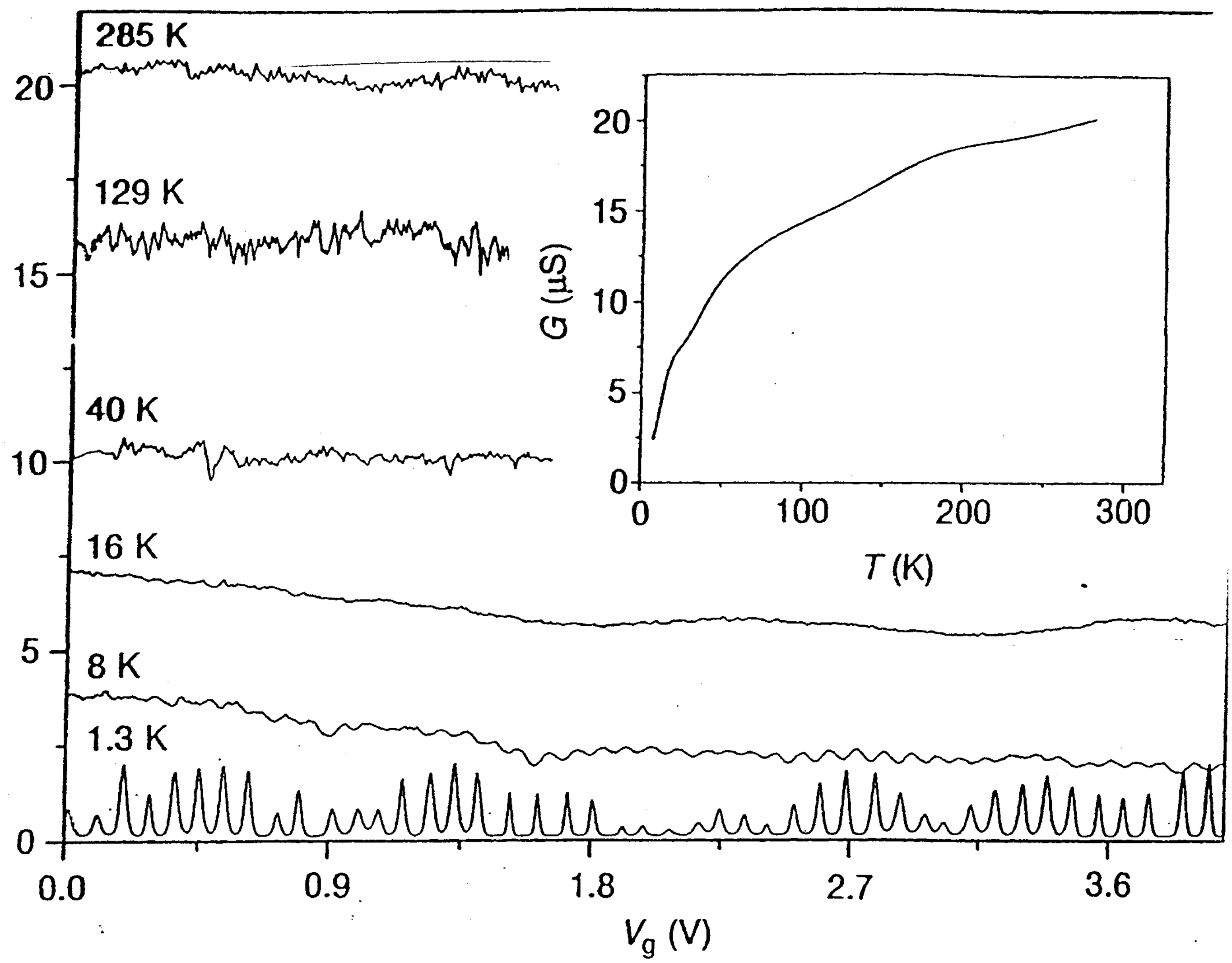

Figure 1 The two-terminal linear-response conductance G versus gate voltag V_g for a bulk-contacted metallic nanotube rope at a variety of temperatures. Th data show significant temperature dependence for energy scales above th charging energy that cannot be explained by the Coulomb blockade mode Inset: average conductance as a function of temperature T. The samples used ir these experiments are made in one of two ways. In both methods, SWNTs are deposited from a suspension in dichloroethane onto a 1-μm-thick layer of SiO_2 that has been thermally grown on a degenerately doped Si wafer, used as a gate electrode. Atomic force microscopy imaging reveals that the diameters of the ropes vary between 1 and 10 nm. In the first method[9], chromium-gold contacts are applied over the top of the nanotube rope using electron beam lithography and lift-off. From measurements of these devices in the Coulomb blockade regime, we conclude that the electrons are confined to the length of rope between the leads. This implies that the leads cut the nanotube ...

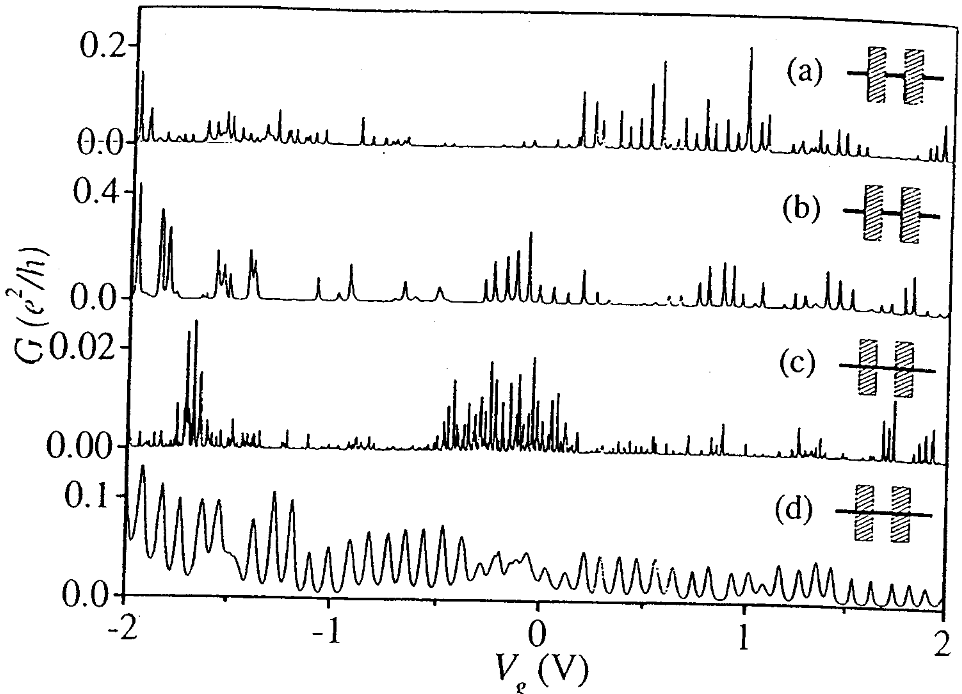

Fig. 4. $G - V_g$ for several devices at 4.2 K. As indicated by the *insets*, (a) and (b) are metal-on-tube, while (c) and (d) are tube-on-metal devices. Note that the oxide thickness is 350 nm for (a)–(c) and 1000 nm for (d)

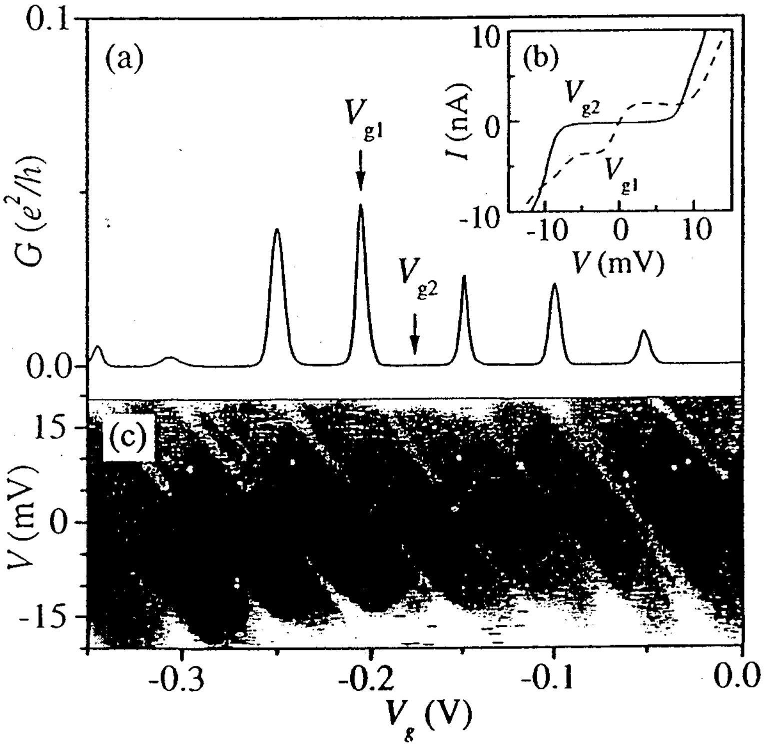

Fig. 5. **a** $G - V_g$ for a device at 4.2 K showing a regular series of CB peaks. **b** $I - V$ characteristics taken at the center of a peak (V_{g1}) and in between peaks (V_{g2}). **c** Grey scale (bias spectroscopy) plot of dI/dV vs. V_g and V at 4.2 K in the same range of V_g (lighter = more positive)

more between devic
to charging the full
that the electron stat
over the contacts.

Figure 6 shows
ture further, to 100 r
metal-on-tube devic
corresponding to the
peaks are now sharp
by device noise rathe
spectroscopy plot of
R. The lines corresp
very sharp.

A magnetic field
is expected to modi
Bohm type phase [3
deed recently been r
tubes in this geomet
ever too small for t
where the flux linke
ing a radius $r = 7$ Å)

Nygard, et al, '99

Scaling

For a weak link tunnelling conductance

$$G(V,T) = AT^{\alpha} \cosh\left(\frac{eV}{2k_B T}\right) \left| \Gamma\left(\frac{1+\alpha}{2} + \frac{ieV}{2\pi k_B T}\right)\right|^2$$

scaling function

V - voltage drop across the link
T - temperature

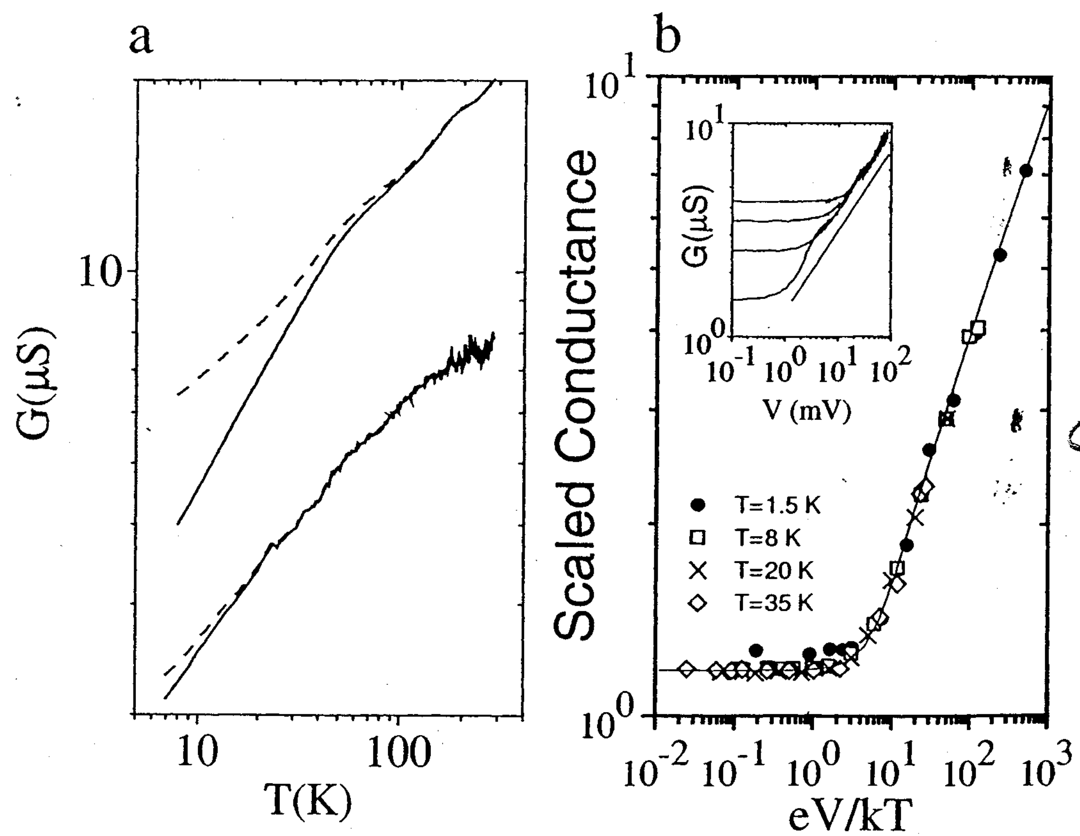

Fig. 7. (a) Conductance plotted against temperature on a double-logarithmic scale

from Bockrath et al. Nature (1999)

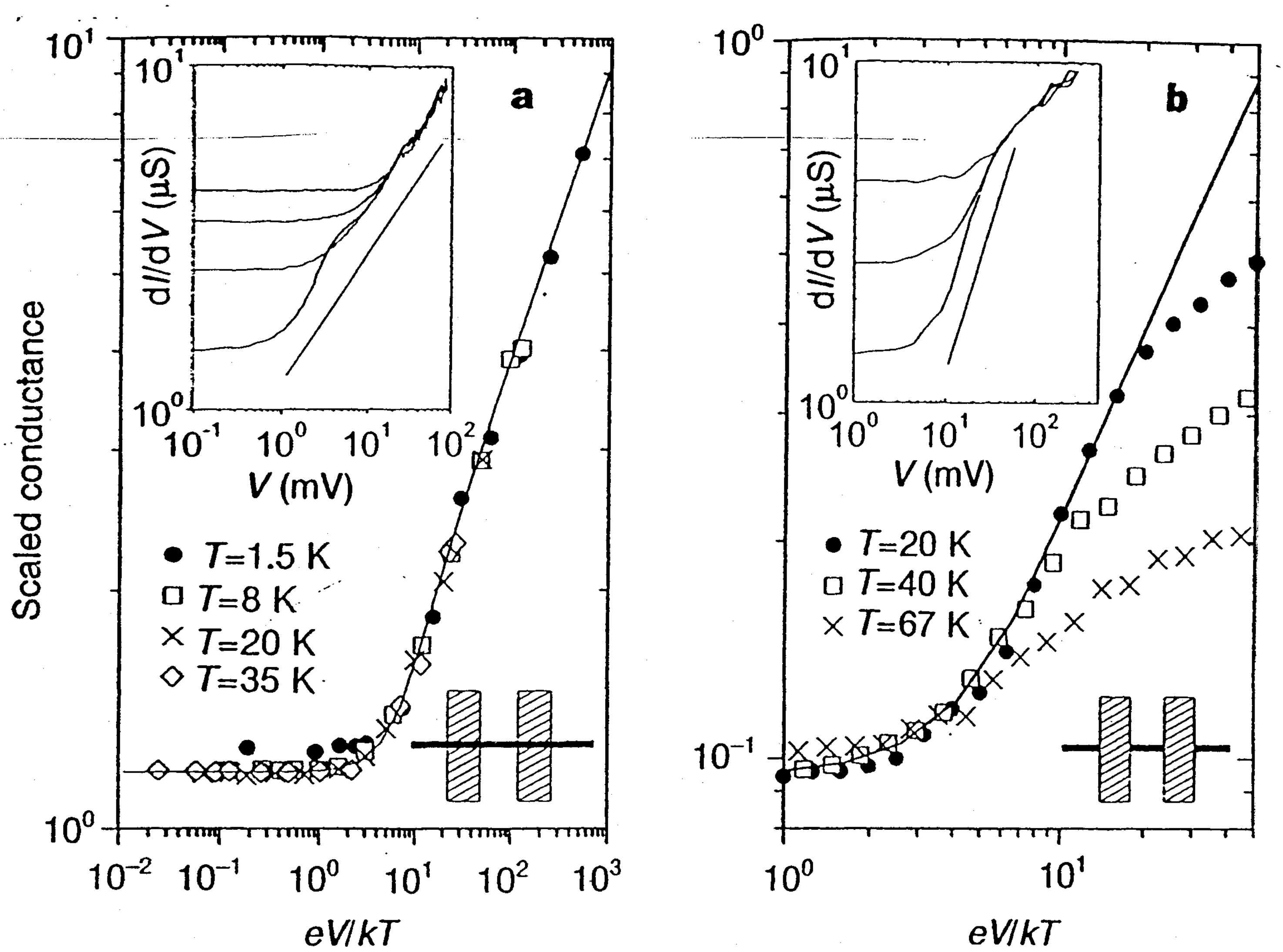

igure 3 The differential conductance dI/dV measured at various temperatures. nset in **a**, dI/dV curves taken on a bulk-contacted rope at temperatures $T = 1.6$ K, K, 20 K and 35 K. Inset in **b**, dI/dV curves taken on an end-contacted rope at emperatures $T = 20$ K, 40 K and 67 K. In both insets, a straight line on the log-log lot is shown as a guide to the eye to indicate power-law behaviour. The main anels **a** and **b** show these measurements collapsed onto a single curve by using he scaling relations described in the text. The solid line is the theoretical result itted to the data by using γ as a fitting parameter. The values of γ resulting in the est fit to the data are $\gamma = 0.46$ in **a** and $\gamma = 0.63$ in **b**.

Crossed set-up

(Komnik & Egger PRL (1998))

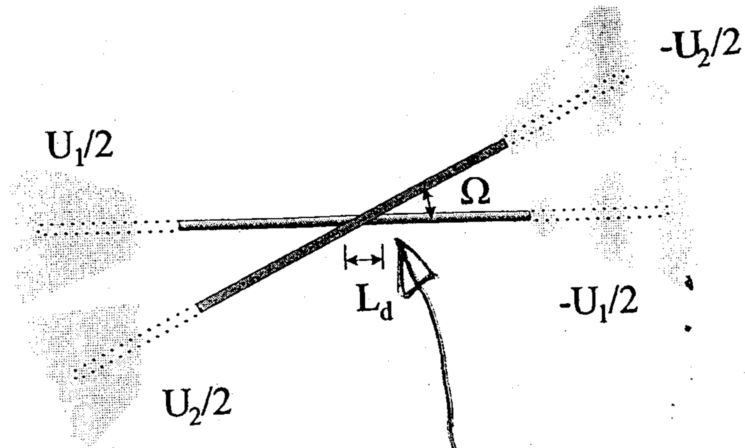

The only important interaction at the contact:

$$H_{int} = \lambda \cos\left[\sqrt{4\pi g}\, \Phi_1(0)\right] \cos\left[\sqrt{4\pi g}\, \Phi_2(0)\right]$$

In the relative channels, $\Phi_{\pm} = \frac{1}{\sqrt{2}}\left[\Phi_1 \pm \Phi_2\right]$, this decouples into two Sine-Gordon models:

$$H_{\pm} = H_0\left[\phi_{\pm}\right] \pm (\lambda/2) \cos\left[\sqrt{8\pi g}\, \Phi_{\pm}(0)\right] \leftarrow \text{solvable}$$

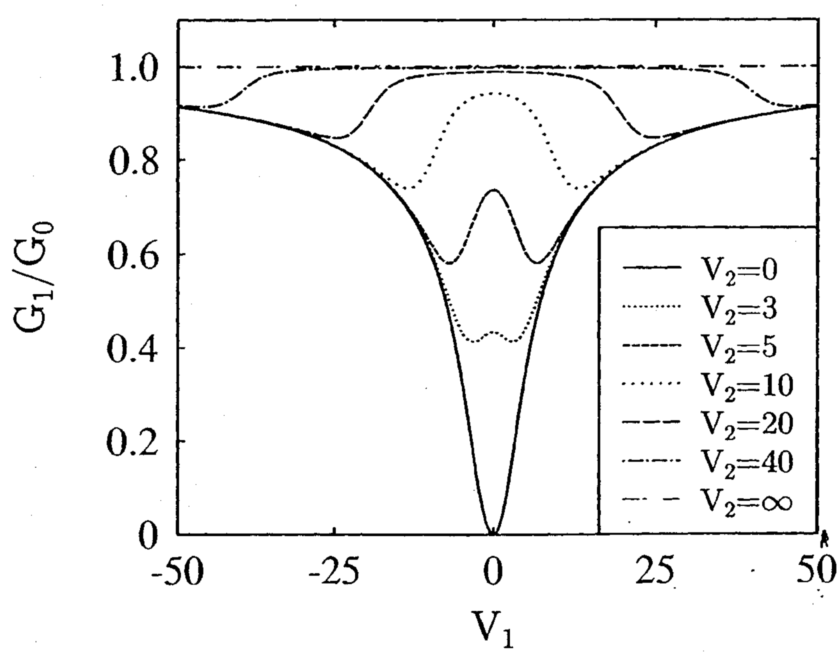

Fig. 3. Conductance $G_1/G_0 \equiv I_1/(e^2V_1/h)$ for $g = 1/4, T = 0$, and several values of the cross voltage V_2. The overall energy scale is set by the coupling λ.

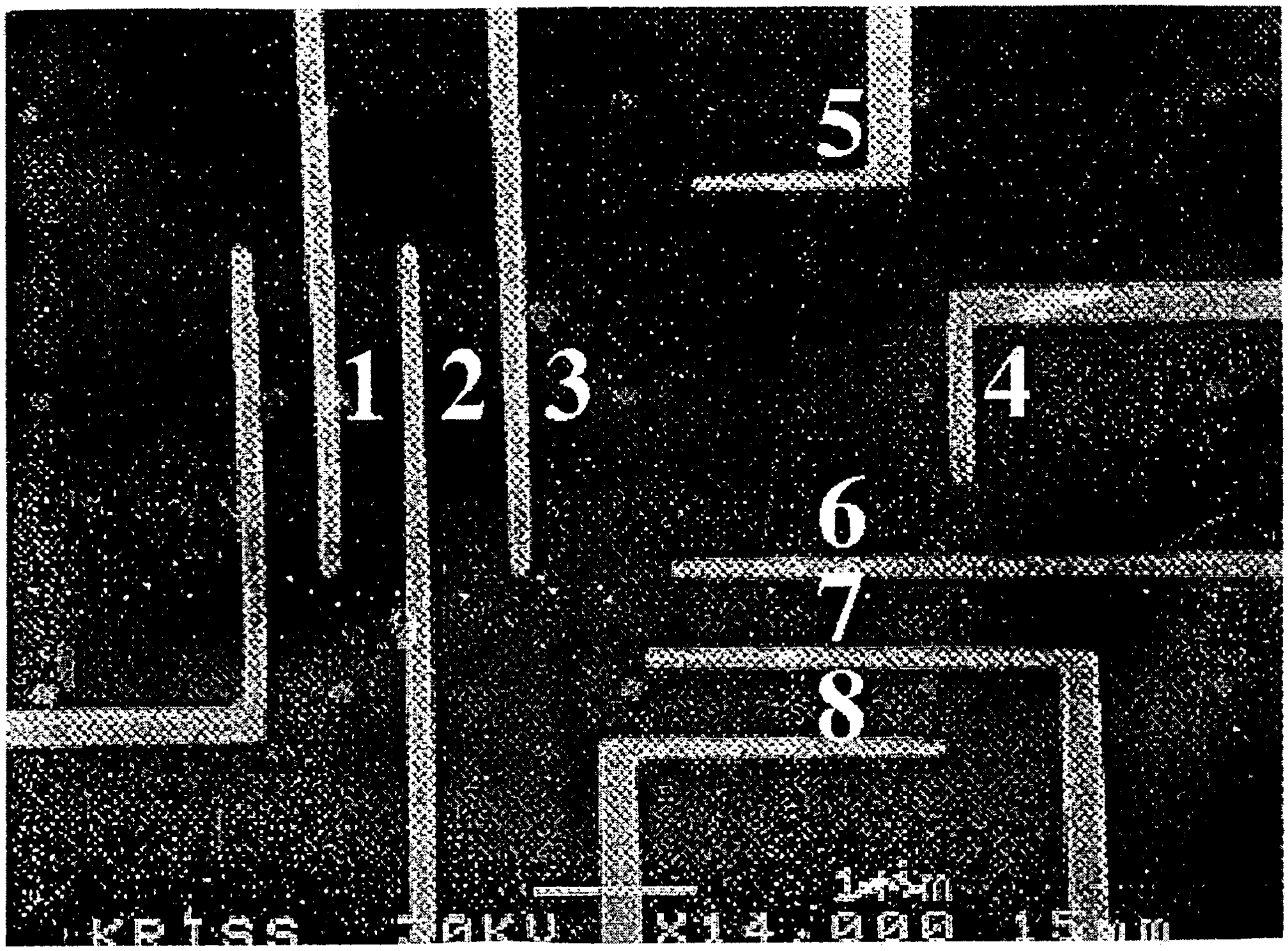

From Kim et al. cond-mat/0005083.

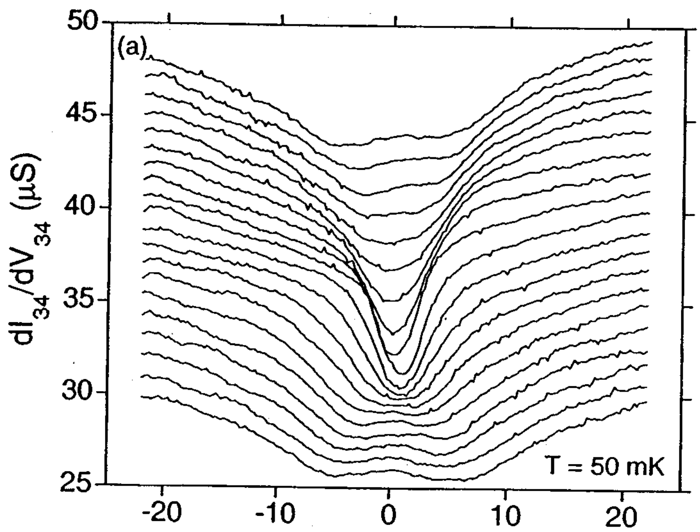

G. & Komnik
cond-mat/0106448

Field emission

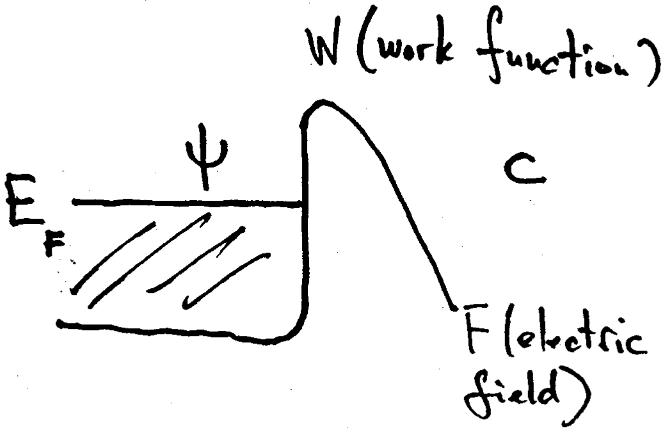

$$H = H_0[c] + H_{LL}[\psi] + \underbrace{\gamma}_{\text{tunnelling}} \left[\psi^\dagger(0)c(0) + c^\dagger(0)\psi(0)\right]$$

<u>Energy resolved</u> current $\longrightarrow$ $J(\omega) = \mathcal{F}\mathcal{D}(\omega)n(\omega)$

$\mathcal{F}$ is the form factor of the emitter, $n(\omega)$ is the energy distribution function of the electrons in the emitter and $\mathcal{D}(\omega)$ is the transmission coefficient of the barrier. For the triangularly-shaped one

$$\mathcal{D}(\omega) \sim \exp(-4\sqrt{2m}(W-\omega)^{3/2}/3\hbar F)$$

At lowest order in γ: $n(\omega)$ – <u>equilibrium</u> distribution

In the case of Luttinger liquids:

$$n(\omega) = \Theta(E_F - \omega)|\omega - E_F|^{1/g-1}/a_0 D^{1/g}\Gamma(1/g)$$

$\Rightarrow$ sharp edge!

- $J(\omega)$ has exponential behaviour below E_F
- $J(\omega) \sim |\omega - E_F|^{1/g-1}$ in immediate vicinity of E_F
- generalisation of Fowler-Nordheim law to LLs:

$$J = \frac{\mathcal{F}}{a_0 D^{1/g}} \left[\frac{F^2}{4k_F W}\right]^{1/2g} \exp\left(-\frac{4k_F^{1/2}}{3F} W^{3/2}\right)$$

- $J(\omega) = 0$ above E_F

$\rightarrow$ this is in fact not true, hence interactions and higher orders in γ <u>needed</u>

(1)

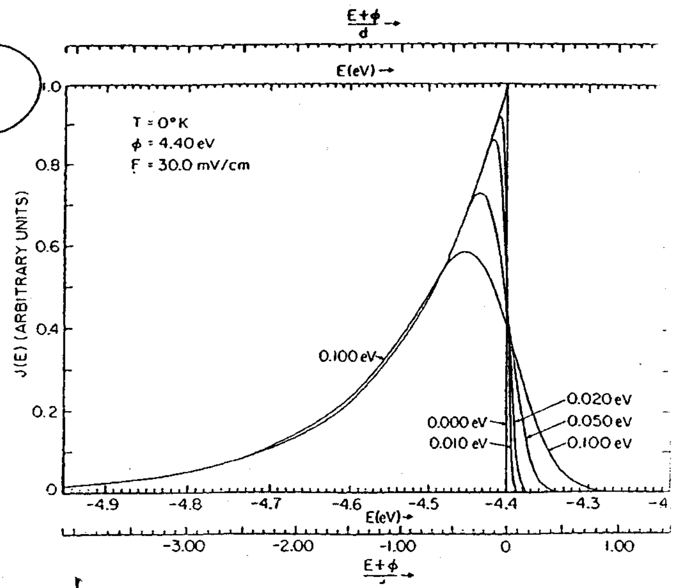

Fig. 7. Theoretical total energy distribution of field emitted electrons from a free-electron metal with various analyzer widths for zero temperature. (YK68.)

(3)

'Secondary current'

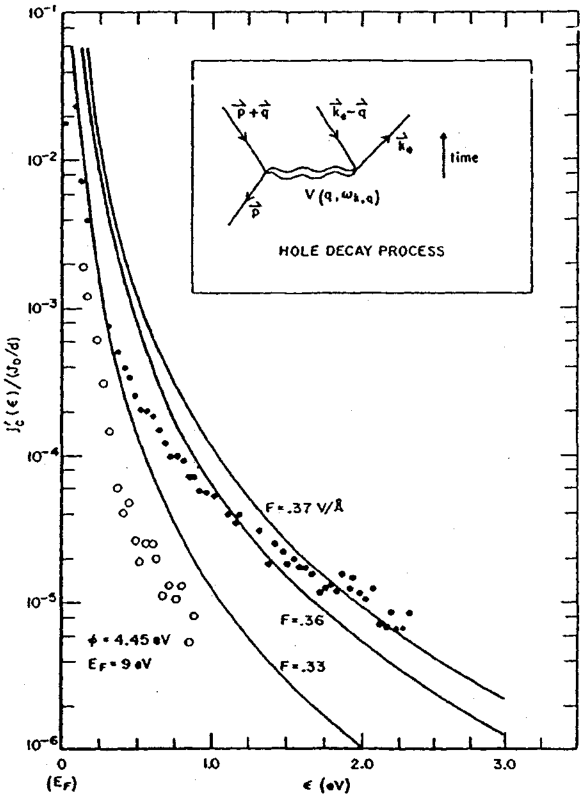

FIG. 2. Solid lines: theoretical calculations for the high-energy tail of the TED for fields 0.33, 0.36, and 0.37 $V/Å$. These curves rise to $dj/d\epsilon = 1$ at $\epsilon = 0$, and then decay exponentially for $\epsilon < 0$ in the well understood way shown in Fig. 1. Closed circles: experimental points for $F = 0.37$ V/Å; open circles: for 0.326 V/Å. Inset: Diagram illustrating the hole-damping mechanism in which a hole of energy-momentum $E_p, \vec{p}$ scatters from the electron gas exciting an electron-hole pair of energy-momentum $\omega_{k,q}, \vec{p}$. The electron momentum is $\vec{k}_\epsilon$.

(2)

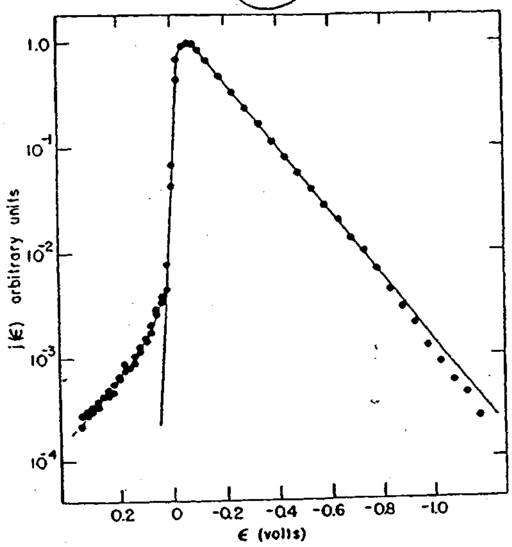

FIG. 2. Total energy distribution from the (120) plane at 20°K, with $F = 0.300$ V/Å and a probe current after multiplication of 1×10^{-8} A. The points are experimental; the line, a convolution of Eq. (1) and a Gaussian analyzer transmission function with a full width at half-maximum of 40 meV.

From Lea & Gomer, PRL (1970)

Qualitative explanation for secondary current:

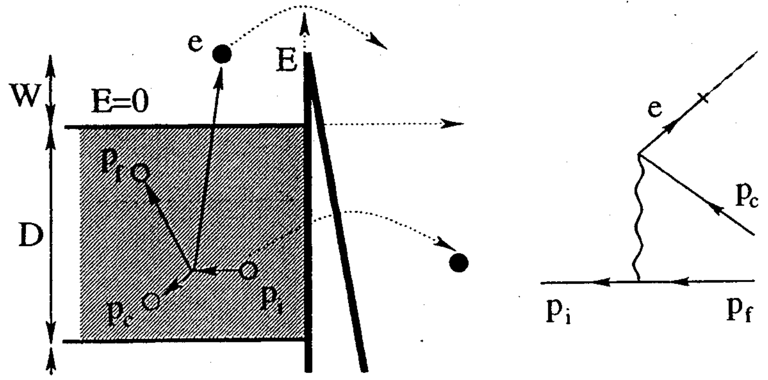

Must calculate GF at the emmiter's tip:

$$\delta g^{-+}(t_1,t_2) = \gamma^2 \int_C dt_3\, dt_4\, \mathcal{K}_C(t_1^-, t_2^+; t_3, t_4) G(t_3, t_4)$$

where $\mathcal{K}_C(t_1^-, t_2^+; t_3, t_4) = \langle T_C[\psi^\dagger(t_2^+)\psi^\dagger(t_3)\psi(t_4)\psi(t_1^-)]\rangle$ and $G(t_3,t_4)$ is the corresponding Green's function of c-operators

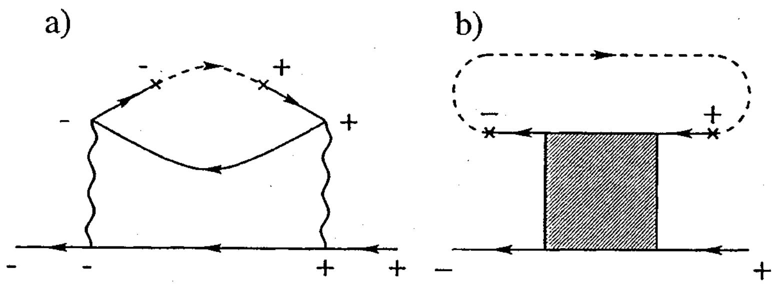

Spectral analysis:

$$j(\omega > E_F) \propto \lim_{V_b\to\infty} \int_{-\infty}^{\infty} dt \frac{e^{i(\omega - E_F - V_b)t}}{t + i\alpha} \int_0^\infty d\tau_1 \int_0^\infty d\tau_2 e^{i(\omega - E_F)(\tau_1+\tau_2)}$$
$$\times \langle \{\psi^\dagger(\tau_1), \psi^\dagger(0)\}\{\psi(t+\tau_1), \psi(t+\tau_1+\tau_2)\}\rangle .$$

Braiding

Luttinger braiding $\psi(t_1)\psi(t_2) = e^{i\pi \mathrm{sign}(t_1-t_2)/g}\psi(t_2)\psi(t_1)$, so

- $j(\omega > E_F) \sim \left(\frac{\omega - E_F}{D}\right)^\lambda$, where $\lambda = 1/g - 2$

- for single-wall carbon nanotubes substitute $1/g$ by $(1/K+3)/4$, so

divergent 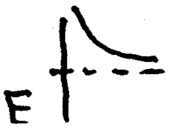 / Convergent 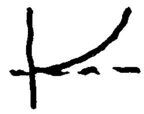 threshold is $K_c = 1/5$

23

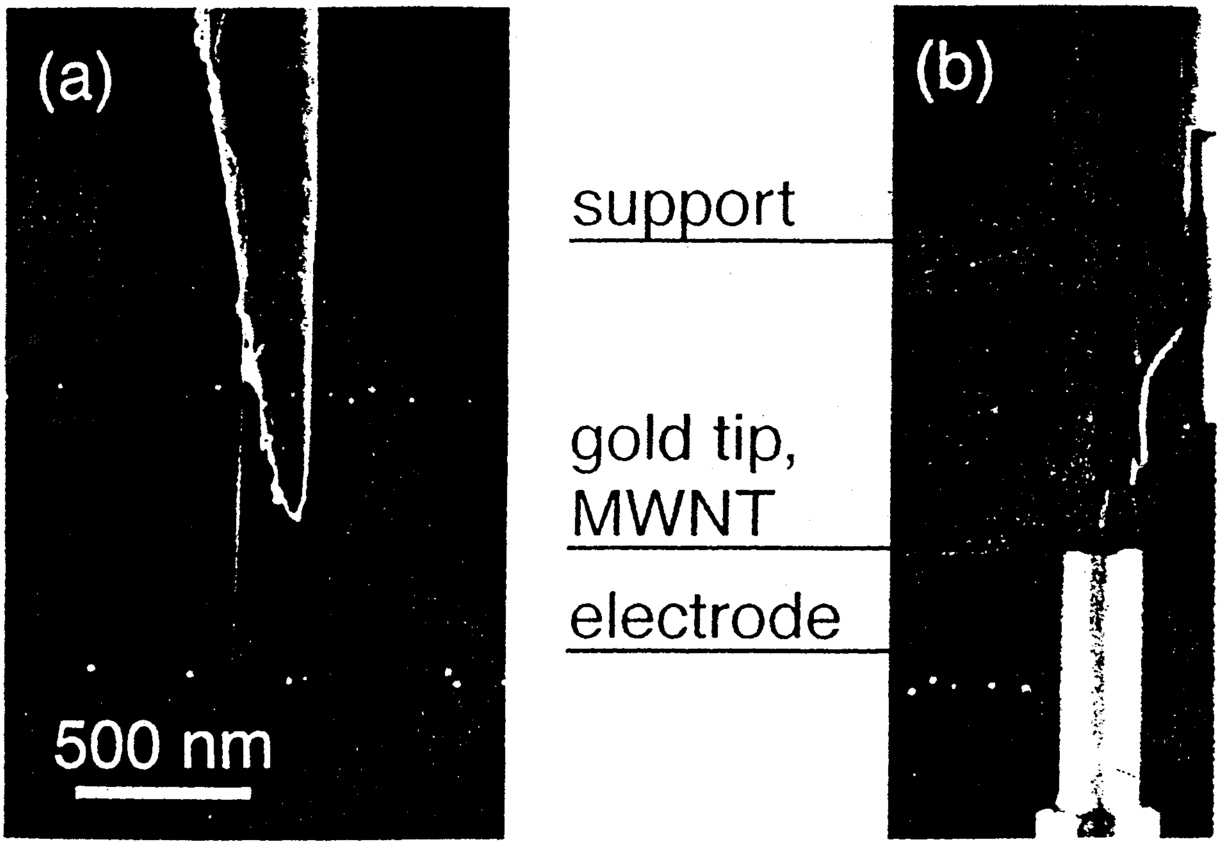

Fig. 2. **a** Single MWNT mounted on the tip of an etched gold \
b Optical micrograph of the experimental setup for field emission: th
wire is fixed on a support, and placed 1 mm above the cylindrical co
electrode

From Bouard et al.
Appl. Phys (1999)